On the Phase Relations and Structural and Magnetic Properties of the Stable Manganese Carbides $Mn_{23}C_6$, Mn_5C_2 and Mn_7C_3

P. Karen,[a] H. Fjellvåg,[b] A. Kjekshus[b,*] and A. F. Andresen[c]

[a] Department of Inorganic Chemistry, Prague Institute of Chemical Technology, CS-16628 Praha 6, Czechoslovakia, [b] Department of Chemistry, University of Oslo, Blindern, N-0315 Oslo 3, Norway and [c] Institute for Energy Technology, N-2007 Kjeller, Norway

Karen, P., Fjellvåg, H., Kjekshus, A. and Andresen, A. F., 1991. On the Phase Relations and Structural and Magnetic Properties of the Stable Manganese Carbides $Mn_{23}C_6$, Mn_5C_2 and Mn_7C_3. – Acta Chem. Scand. 45: 549–557.

Single phase samples of the manganese carbides $Mn_{23}C_6$, Mn_5C_2 and Mn_7C_3 were prepared, and examined by powder X-ray and neutron diffraction at various temperatures. In the case of Mn_7C_3, a chemical transport technique was developed to achieve well crystallized samples of at least 99 % phase purity. The thermal stability of $Mn_{23}C_6$ (and $Mn_{15}C_4$) is found to be higher than earlier reported, since Mn_4C_{1+x} could not be obtained by quenching from temperatures up to 1250 °C. Improved unit cell parameters and thermal expansion data are given for the carbides. Refined atomic coordinates from powder neutron diffraction data permit a confirmation of isostructurality with the structure prototypes $Cr_{23}C_6$, Pd_5B_2, Cr_7C_3 and comparisons of structural and bonding features for the three carbide phases. Owing to the small atomic size of Mn, as compared with Pd and Cr, carbon exhibits higher coordination numbers in Mn_5C_2 and Mn_7C_3 than in the prototypes. Monocapped trigonal prisms are found in Mn_5C_2, and coordination numbers 7 and 8 can be assigned to the carbon coordination polyhedra in the Mn_7C_3 structure. As the carbon content increases in the sequence $Mn_{23}C_6$, Mn_5C_2 and Mn_7C_3, the Mn–C bond order increases (average Mn–C distance 211, 208 and 208 (206) pm, respectively) and the Mn–Mn bond order decreases (average Mn–Mn distance 261.6, 263.8 and 264.5 pm, respectively). The closest C–C separation (335, 312 and 295 pm, respectively) is believed to be caused by the geometry of the structures, and consequently the possibility of direct C–C bonding interaction is excluded. The three carbides are weak paramagnets at ambient temperature. For $Mn_{23}C_6$, Curie–Weiss behaviour is observed with $\Theta_p = +38 \pm 3$ K, and $\mu_{eff} = 1.46 \pm 0.02$ μ_B. Neutron diffraction data show that $Mn_{23}C_6$ is magnetically ordered below $T_N = 104 \pm 2$ K. No indications of magnetic order were found for Mn_5C_2 and Mn_7C_3 at temperatures above 16 K.

Few classes of transition metal compounds change their properties so extensively throughout the 3*d* series as the carbides. The difference between the hard, refractory carbides of Ti and V and the highly unstable carbides of Ni, Cu and Zn is quite remarkable. Owing to the position of Mn in the middle of the 3*d* series, the manganese carbides exhibit a large variety of properties. They are hard and brittle,[1] but their thermal stability generally does not exceed 1000–1100 °C.[2] On the other hand, although the Mn–C system is rather complex at elevated temperature, only $Mn_{23}C_6$, Mn_5C_2 and Mn_7C_3 are claimed[2–4] to be thermodynamically stable at ambient temperatures. The coordination of carbon in the crystal structures of the manganese carbides resembles the structural features of the iron group carbides.[5,6] The presence of uncompensated spins gives rise to paramagnetic behaviour.[7] Unlike the carbides of all the other 3*d* metals, the manganese carbides are readily hydrolyzed by water or atmospheric moisture.[8–11]

The structures of the manganese carbides have never been properly verified. However, the structure prototypes, i.e. $Cr_{23}C_6$ (Ref. 11), Pd_5B_2 (Ref. 12) and Cr_7C_3 (Ref. 13), are well determined by single-crystal X-ray diffraction, and the isostructurality of the manganese carbides is supposed[11–18] on the basis of similarity in the powder X-ray diffraction (PXD) patterns. For $Cr_{23}C_6$, a structure refinement based on powder neutron diffraction (PND) data is also available,[19] and a recent study[20] discusses the defect structure of $(Cr,Fe)_7C_3$ as studied by X-ray diffraction and high resolution electron microscopy (HREM).

As a consequence of their low thermal and chemical stability, manganese carbides are rarely prepared in phase pure or chemically pure form. They exhibit an apparent tendency to accommodate significant amounts of dissolved oxygen[2] or nitrogen,[21] features which subsequently influence their properties. On this background it is perhaps quite understandable that of the twelve differently claimed manganese carbides, only six have later been confirmed (see, e.g., Ref. 17 and references therein).

The present article aims at providing a consistent study of structural and magnetic properties of the stable Mn–C phases. Low- and high-temperature PXD and PND techniques are used to investigate samples for which strict precautions were taken in order to avoid contamination.

* To whom correspondence should be addressed.

Experimental

Manganese discs (99.9 % Mn, Ventron GMBH) were surface cleaned in 80 % formic acid, washed in methanol–n-hexane mixtures with gradually increasing portions of n-hexane, dried and crushed in a flow of dry argon. The manganese powder (particle size ~0.7 mm) and carbon powder (spectral graphite, Elektrokarbon Topolčany, Czechoslovakia) were homogenized in an agate rotational ball mill under dry benzene for 2 h. The resulting grey slurry was pressed into cylindrical pellets of 8 mm diameter. After drying in a desiccator (P_2O_5 and foamed polystyrene as drying agents), the pellets were placed in a molybdenum container which in turn was sealed in a silica glass ampoule under a pressure of ~10 Pa. The residual atmosphere in the ampoule was gettered by help of freshly cut pieces of Misch Metal ("*Ber*", Treibacher, Austria), situated in a separate corundum crucible. The heat treatment involved short-term local heating of the getter (2 h, 900 °C) and long-term heating of the whole ampoule (200–250 h, 900 °C).

For the preparation of the most carbon-rich manganese carbide, Mn_7C_3, an additional 20 % carbon was introduced into the ampoule (using only 90 % of the stoichiometric amount of C in the pellets) either in the form of vitreous carbon or as spectral carbon soaked with ~3 wt. % of paraffin oil. The temperature gradient along the ampoule did not exceed 50 °C, the getter and "surplus" carbon part being kept at the high-temperature end.

PXD data were collected at room temperature with a Guinier camera ($CrK\alpha_1$ radiation, $\lambda = 228.962$ pm; Si as internal standard, $a = 543.054$ pm). The positions and integrated intensities of the Bragg reflections were evaluated from the films using a Nicolet L18 scanner and the SCANPI[22] program system. Low- and high-temperature PXD data were obtained from 90 to 300 and 300 to 1300 K, respectively, using an Enraf–Nonius camera of the Guinier–Simon type ($MoK\alpha_1$ radiation, $\lambda = 70.926$ pm). The unit cell parameters were calculated by least-squares refinements.[23]

PND data were collected with the OPUS III diffractometer (at the JEEP II reactor, Kjeller) at temperatures between 10 and 300 K (Displex cooling unit) using neutrons of wavelength of 187.7 pm. Approximately 6 cm^3 of a coarsely pulverized sample was placed into a vanadium sample holder under a He atmosphere, and the diffraction data were collected in steps of 0.05° between 5 and 100° in 2θ.

Atomic coordinates were refined according to the Rietveld method,[24] using the Hewat[25] version of the program. The scattering lengths of Mn and C, $b_{Mn} = -3.73$ fm and $b_C = 6.65$ fm, respectively, were taken from Ref. 26. The unit cell parameters, scale factor, zero point and half-width parameters were refined, together with atomic coordinates and isotropic temperature factors. However, no corrections for neutron absorption were performed, and by neglecting this, some temperature factors obtained a slightly negative value.

Magnetic susceptibility data were recorded between 80 and 1000 K using a Faraday balance. The samples were contained in vacuum-sealed silica glass ampoules during the measurements. Low-temperature susceptibility data for $Mn_{23}C_6$ were also obtained between 54 and 250 K by an a.c. induction method. The sample chamber inside the field coil (4.4 kOe) was cooled by liquid nitrogen and the induced voltage in the pick-up coils was measured by an EG&G model 5104 lock-in voltmeter combined with an ultra-low-noise preamplifier EG&G 5004.

Results and discussion

Syntheses and phase relations. Two problems concerning phase purity are frequently encountered during the synthesis of manganese carbides: (i) partial formation of another manganese carbide (or degradation to the metal) and (ii) contamination by oxygen which manifests itself ultimately as MnO.

As the carbon content is only slightly different for the various manganese carbides, any imbalance in the Mn to C ratio will contribute significantly to a distribution of carbide phases in the product. Among the many possible causes for such a bulk imbalance, the most common one is contamination by oxygen during the preparation. The high affinity of manganese towards oxygen results *inter alia* in reaction between the metal and the silica glass, which must be prevented by using a suitable container during the closed ampoule syntheses. However, a local imbalance in the Mn/C ratio can still be created by various transport reactions inside the ampoule, as will be discussed later.

For Mn_7C_3, a complete phase purity as seen by PXD was achieved on adopting the chemical transport technique (facilitated by the fact that Mn_7C_3 is the most carbon-rich carbide of manganese). From a series of blank experiments it was established that the presence of minute amounts of hydrogen (say 10^{-3} mol per mol Mn), in addition to the surplus carbon in the ampoule, is a prerequisite for a massive carbon transport via the gas phase. Presumably, hydrocarbons (say CH_4 or C_2H_4) or hydrocarbon radicals serve as transporting agents, in a similar manner to their role during the reactions of manganese with hydrocarbons in open systems.[8,27] Since these reactions proceed at temperatures as low as 700 °C (Refs. 27 and 28), the exact temperature does not represent any strict precondition for the successful transport synthesis of Mn_7C_3 (which is claimed[29] to be stable up to 1340 °C). In addition to the phase-purity advantage, this technique also gives well developed crystallites. Contamination by MnO was usually not observed in the present Mn_7C_3 samples. However, in one (the only) case where this problem occurred, the impurity was concentrated on the part of the sample rod most distant from the getter.

Temperature homogeneity is crucial for the successful syntheses of $Mn_{23}C_6$ and Mn_5C_2. Any presence of traces of water in the reaction vessel will redistribute the carbon content along the temperature gradient of the sample rod.

Several trial-and-error experiments were carried out for optimization of the sample position within the furnace in order to eliminate this problem. With appropriate precautions, Mn_5C_2 and $Mn_{23}C_6$ were obtained as pure carbide phases in amounts sufficient for PND, however, with contamination of MnO in amounts of, respectively, ≤ 1 and ~ 3 %. This finding gives evidence for a very low solubility of oxygen in $Mn_{23}C_6$, and it does not support the proposed[2] existence of $Mn_{23}(C,O)_6$ which was presumed[2] as an oxygen-saturated counterpart to the pure carbide $Mn_{15}C_4$. According to the present findings, the formation of $Mn_{15}C_4$ and $Mn_{23}C_6$ depends exclusively on the carbon content. As the carbon content is increased, the diffraction pattern of the $Mn_{23}C_6$ phase shifts continuously towards the pattern of $Mn_{15}C_4$. A broadening of the lines gives evidence of structural disorder in the transition region. Moreover, as opposed to earlier suggestions,[2] $Mn_{15}C_4$ seems to be fairly stable below 850 °C. This appears to be consistent with the findings of Schuster and Nowotny.[30] It is likely that $Mn_{23}C_6$ and $Mn_{15}C_4$ are to be considered as limiting formulae of a homogeneity region (although with gradual changes in the structural arrangement due to differences in the stacking sequences of the c.c.p. and h.c.p. layers of structural Mn clusters), where they are in equilibrium with Mn and Mn_5C_2, respectively. A PND structural investigation of $Mn_{15}C_4$ is currently in progress.

The $Mn_4C_{1\pm x}$ phase[3] with the ε-Fe_3N type[31] structure was not observed during our numerous experiments. Quenching in water (at a rate of 100 °C s^{-1}; from temperatures up to 1250 °C) of samples with nominal compositions between Mn_5C and $Mn_{23}C_6$ invariably gave mixtures of Mn and $Mn_{23}C_6$. According to these observations, the thermal stability of $Mn_{23}C_6$ must be much higher than the commonly adopted[2,4] limit of 1025 °C. The latter temperature stems from Ref. 2, where it was established from studies on solid solutions of $Mn_{23}C_6$ with its much less stable iron counterpart, $Fe_{23}C_6$. The same argument is valid for the thermal stability of $Mn_{15}C_4$.

It should be mentioned that a sample which showed the characteristic diffraction pattern of an ε-Fe_3N-type phase (admixed with that of Mn_5C_2) was obtained during one of the blank experiments, where the additional carbon was lacking, but hydrogen was abundant in the ampoule during the reaction (see Experimental). The unit cell parameters of this phase [$a = 278.60(4)$ and $c = 450.07(7)$ pm] are close to those earlier reported[3] for Mn_4C_{1+x}. The samples described in Ref. 3 were quenched in water without any protection, which casts some doubts on their subsequent purity. Assuming all these facts, it is inferred that the hexagonal Mn_4C_{1+x} phase is stabilized by another nonmetal.

Structural properties of Mn_7C_3. According to the PXD and PND patterns, the present Mn_7C_3 samples, prepared by chemical transport, have developed a clear and distinct orthorhombic symmetry, as opposed to the hexagonal symmetry caused by disorder which is usually observed when traditional solid-state reaction techniques are used for the preparation of this carbide. The unit cell parameters, $a = 454.30(4)$, $b = 695.44(7)$ and $c = 1197.3(1)$ pm, were derived from 33 reflections and are in close agreement with Ref. 17. The deviation of these unit cell parameters from hexagonality corresponds to $\gamma = 118.8°$. Unequivocally orthorhombic indexable (not pseudo-hexagonal, Ru_7B_3 type) reflections were used to establish the thermal variation of the unit cell parameters over the interval 110 to 1300 K shown in Fig. 1. No indication of any phase transition is found. The thermal expansion is almost linear within the range, and upon such an approximation the linear expansion coefficients are: $\alpha_a = \Delta a/(a\Delta T) = (12.9 \pm 0.6)\times10^{-6}$ K^{-1}; $\alpha_b = (20.4 \pm 1.1)\times10^{-6}$ K^{-1}; $\alpha_c = (19.3 \pm 0.5)\times10^{-6}$ K^{-1}; and $\alpha_V = (54.2 \pm 2)\times10^{-6}$ K^{-1}.

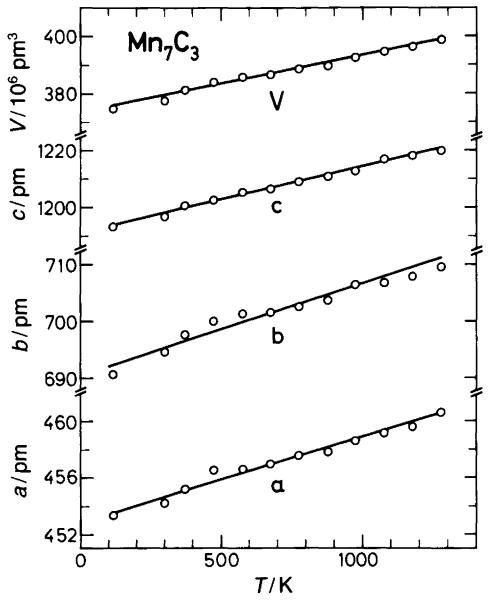

Fig. 1. Variation in unit cell parameters of Mn_7C_3 between 110 and 1300 K.

The unconstrained atomic coordinates derived by profile refinements of the PND data recorded at 298 K are listed in Table 1.

Table 1. Atomic coordinates for Mn_7C_3 at 298 K as derived by Rietveld refinements. Space group *Pnma*; $Z = 4$. Calculated standard deviations in parentheses. Reliability factor for nuclear reflections $R_n = 10$ %.

Atom	Site	*x*	*y*	*z*
Mn_I	8d	0.260(4)	0.050(5)	0.015(3)
Mn_{II}	8d	0.059(4)	0.080(3)	0.804(3)
Mn_{III}	4c	0.275(6)	0.25	0.182(4)
Mn_{IV}	4c	0.280(6)	0.25	0.420(5)
Mn_V	4c	0.097(8)	0.25	0.640(4)
C_I	8d	0.041(2)	0.038(1)	0.354(1)
C_{II}	4c	0.456(4)	0.25	0.556(3)

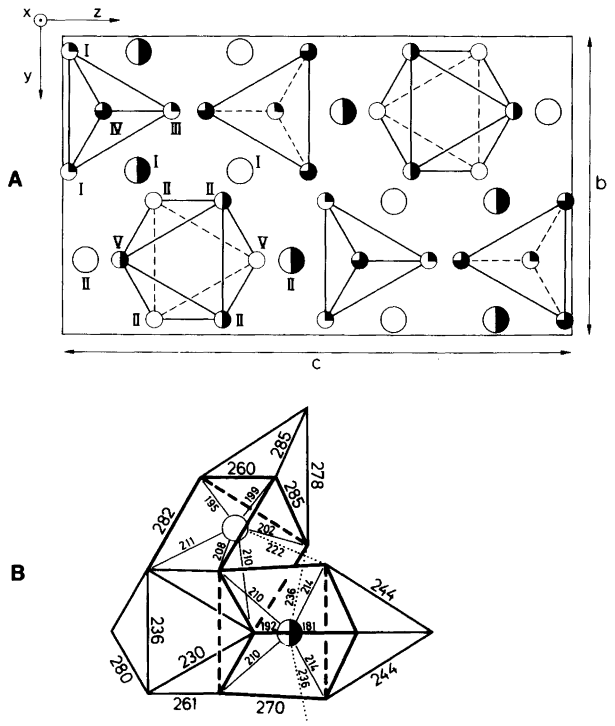

Fig. 2. Structure of Mn_7C_3. (A) Content of orthorhombic unit cell within an idealized structure with pseudo-hexagonal symmetry; smaller circles: Mn, larger circles: C; approximate height above the projection plane shown by degree of filling of circles. Roman characters refer to numbering of atoms (Table 1). (B) Coordination around C_I and C_{II} and neighbouring Mn octahedra and trigonal bipyramides. Approximate interatomic distances (in pm at 298 K) are shown.

The Mn_7C_3 structure can, at first sight, be described as being composed of columns of confacial manganese octahedra and columns of convertical manganese trigonal bipyramids, oriented so that trigonal prismatic voids are formed between both types of columns (Fig. 2A). The relative positioning of the columns implies that three trigonal prismatic voids per octahedron and one trigonal bipyramid are available to accommodate the non-metal. Carbon fills two voids adjacent to one half and one void adjacent to the second half of the trigonal bipyramid, thereby excluding any possible hexagonal symmetry of the structure. In order to allow for the two crystallographically different carbon coordinations, the confacial columns adopt two different orientations. The bipyramidal chains are flattened and deformed in the [001] direction (Fig. 2B), which implies contraction of the orthorhombic *c*-axis and deviation from a hexagonal metric, $c_{orth} \neq \sqrt{3}\, b_{orth}$.

The structural features can best be discussed by comparison with the hexagonal structure of Ru_7B_3,[32] in which all the octahedral columns have the same orientation. Let the hexagonal framework of metal atoms in Ru_7B_3 be further idealized by supposing all the closest metal–metal contacts equal. The density of packing of such equal spheres is 0.694, and the arrangement obeys the geometrical condition $c_{hex}/a_{hex} = 2\times\sqrt{2}/(3+\sqrt{3}) \approx 0.598$. Pairs of closely adjacent and tilted trigonal prismatic voids are formed, and therefore only one void for the pair can be filled by the B atoms. If so, the three prisms positioned on the same half (latitude) of the trigonal bipyramid are occupied and rectified (on account of the three remaining non-filled voids), giving also an extension of the six-fold axis. Ru_7B_3 then attains the axial ratio $c_{hex}/a_{hex} = 0.631$. If Ru is exchanged by the smaller Cr and B by the larger C, the equi-latitudinal filling of the voids is not favourable, an additional extension and a rearrangement into orthorhombic symmetry of the Mn_7C_3 structure occurs in Cr_7C_3,[13] and $a_{orth}/b_{orth} = 0.646$. However, the metric remains hexagonal. Because the Mn atom is even smaller than Cr in carbides, a further extension of the columns occurs in Mn_7C_3 to accommodate carbon, and the axial ratio increases to 0.653. The extension along the columns is compensated by an anisotropic contraction of the b_{orth} and c_{orth} axes, and thus also the lattice metric becomes orthorhombic in Mn_7C_3.

The difference in size between Mn and C is also reflected in the carbon coordination. In addition to the conventional trigonal prismatic Mn–C contacts, other contacts (at 222 and 236 pm; Fig. 2B) are observed, which are too close to be assigned as secondary "bonds". Coordination numbers 7 and 8 describe better the reality around the C_I and C_{II} atoms, respectively, although the two contacts to C_{II} at 236 pm are rather ambiguous in this respect. In Cr_7C_3, these secondary contacts are 247 and 246 pm distant from C_I and C_{II}, respectively, whereas the six metal–carbon distances within the conventional trigonal prism are virtually the same for Cr_7C_3 and Mn_7C_3. In accordance with the extensive deformation of the ideal metal framework, a large span also occurs in the Mn–Mn distances within the Mn coordination polyhedra, as is summarized in Table 2.

The closest C–C distance, 295(2) pm, in the structure is considered too long to be ascribed to bonding interaction.

Table 2. Coordination (listed atom to Mn) in Mn_7C_3 and distances (in pm) at 298 K. d_{nb} = shortest contact considered as *non-bonding*, d_{span} = span of bonding contacts, d_{av} = arithmetic average of bonding contacts.

Atom	CN	d_{nb}	d_{span}	d_{av}
Mn_I	11	367	232–285	262.2
Mn_{II}	11	353	230–282	263.7
Mn_{III}	11	356	244–285	269.4
Mn_{IV}	12	373	238–285	268.3
Mn_V	11	348	230–280	261.9
Mn_{av}	11.14	348	230–285	264.5
C_I	7	275	195–222	206.9
C_{II}	8	308	181–236	211.6
C_{II}[a]	6	236	181–214	203.5
C_{av}	7.33	275	181–236	208.4
C_{av}[a]	6.67	236	181–222	205.8

[a] Alternative interpretation, see text.

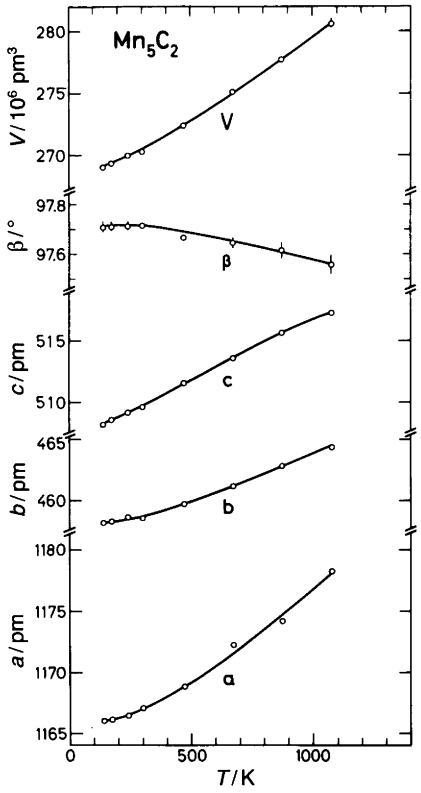

Fig. 3. Variation in unit cell parameters of Mn_5C_2 between 140 and 1100 K. Standard deviations do not exceed half the size of the symbol, except for β and *V*, where exceeding errors are marked with bars.

Structural properties of Mn_5C_2. The unit cell parameters of the monoclinic Mn_5C_2 phase were calculated using only unambiguously indexable reflections from different sets of X-ray data for five independent, phase pure samples. Based on these data, averaged in terms of $\sin^2\theta$, the following values for unit cell parameters were obtained: $a = 1167.24(6)$; $b = 458.64(2)$; $c = 509.69(2)$ pm and $\beta = 97.719(3)°$. These values agree with published data.[15,17,33] The unit cell parameters (and volume) between 300 and 1100 K are plotted in Fig. 3. Linear regression yields the following expansion coefficients: $\alpha_a = (12.1 \pm 0.8) \times 10^{-6}\,K^{-1}$; $\alpha_b = (16.3 \pm 0.4) \times 10^{-6}\,K^{-1}$; $\alpha_c = (19.5 \pm 0.6) \times 10^{-6}\,K^{-1}$; $\alpha_\beta = (-1.9 \pm 0.2) \times 10^{-6}\,K^{-1}$; $\alpha_V = (49.7 \pm 0.9) \times 10^{-6}\,K^{-1}$. As for Mn_7C_3, the highest thermal expansion occurs in the direction along the three-fold axis of the trigonal prismatic part of the carbon coordination polyhedra.

Table 3. Atomic coordinates for Mn_5C_2 at 298 K as derived by Rietveld refinements. Space group *C2/c*; $Z = 4$. Calculated standard deviations in parentheses. $R_n = 9\,\%$.

Atom	Site	*x*	*y*	*z*
Mn_I	8f	0.099(1)	0.093(2)	0.436(3)
Mn_{II}	8f	0.222(1)	0.596(2)	0.300(2)
Mn_{III}	4e	0	0.591(3)	0.25
C_I	8f	0.1123(6)	0.3040(16)	0.0743(16)

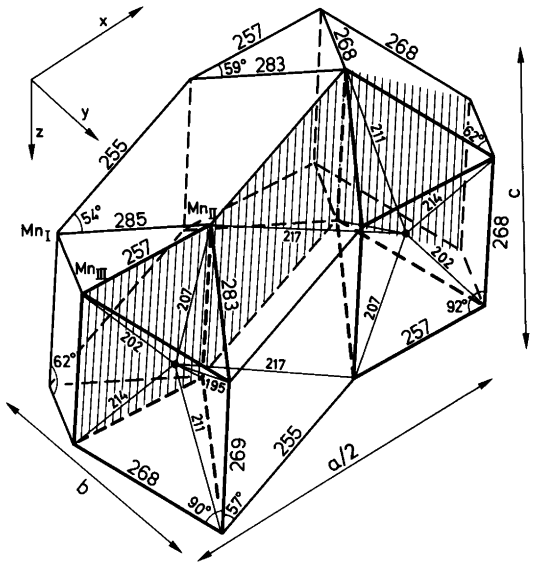

Fig. 4. Structure of Mn_5C_2. Schematic view of one quarter of the unit cell. Interatomic distances (in pm at 298 K) are indicated. Numbering of Mn atoms refers to Table 3.

The unconstrained atomic coordinates of the Mn_5C_2 structure, as refined by the Rietveld method from PND data at 298 K, are listed in Table 3. A representative part of the Mn_5C_2 structure is shown in Fig. 4. The Mn_5C_2 structure shown in Fig. 4 is formally divided into trigonal prismatic and distorted rhombohedral building units. One half of the prisms is tilted, and the second half, which is regular, contains carbon. However, as clearly seen, a seventh Mn–C contact exists at a separation of 217 pm, which is well within the possible scatter of the Mn–C bond distances. The coordination polyhedron of carbon in Mn_5C_2 is therefore better described as a monocapped trigonal prism, which is shown in Fig. 5 with all interatomic distances marked. In this respect, Mn_5C_2 differs from its structural prototype, Pd_5B_2 (Ref. 12), where the corresponding

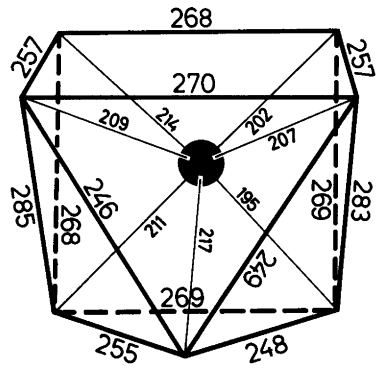

Fig. 5. Carbon coordination polyhedra in Mn_5C_2; distances in pm at 298 K.

Table 4. Coordination (listed atom to Mn) in Mn_5C_2 and distances (in pm) at 298 K. d_{nb} = shortest contact considered as *non-bonding*, d_{span} = span of bonding contacts, d_{av} = arithmetic average of bonding contacts.

Atom	CN	d_{nb}	d_{span}	d_{av}
Mn_I	12	377	248–285	266.9
Mn_{II}	11	351	246–285	260.9
Mn_{III}	10	359	255–269	263.3
Mn_{av}	11.20	351	246–285	263.8
C	7	264	195–217	207.9

seventh distance is 260 pm and correctly is interpreted as a secondary contact. This difference illustrates the size disparity between Mn and Pd, which apparently enables carbon to coordinate more Mn atoms.

The variation in the shortest Mn–Mn distances is smaller in Mn_5C_2 than in Mn_7C_3, but is still considerable, as seen from Table 4. The shortest C–C distance, 312(2) pm, is significantly longer than in Mn_7C_3 and cannot be considered as bonding.

Structural properties of $Mn_{23}C_6$. The unit cell parameter a for the cubic $Mn_{23}C_6$ phase was calculated using three sets of 14 reflections for independent samples where $Mn_{23}C_6$ was in equilibrium with minute amounts of metallic Mn, but with no other carbide present. The value obtained, a = 1059.5(2) pm, fits the results of the precise study reported in Ref. 17. The thermal expansion function is curved in the interval between 80 and 1300 K (Fig. 6), but above 500 K it can be approximated as linear, with $\alpha_a = (18.1 \pm 0.3) \times 10^{-6}\ K^{-1}$.

The unconstrained atomic coordinates at 298 K, as refined by the Rietveld method, are listed in Table 5, and

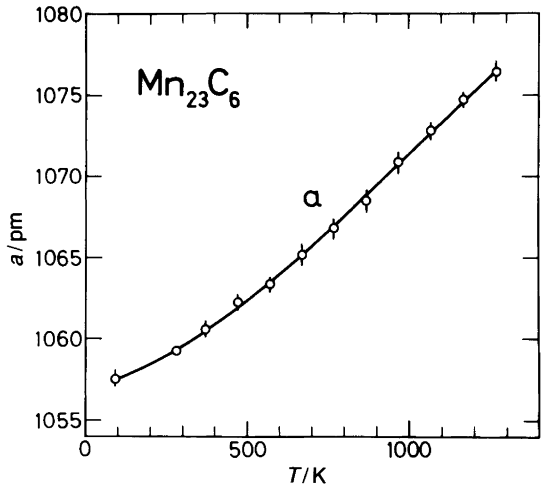

Fig. 6. Variation in unit cell parameter of $Mn_{23}C_6$ between 80 and 1300 K.

Table 5. Atomic coordinates for $Mn_{23}C_6$ at 298 K as derived by Rietveld refinements. Space group *Fm3m*; Z = 4. Calculated standard deviations in parentheses. R_n = 8 %.

Atom	Site	x	y	z
Mn_I	4a	0	0	0
Mn_{II}	8c	0.25	0.25	0.25
Mn_{III}	48h	0	0.1691(2)	0.1691(2)
Mn_{IV}	32f	0.3820(3)	0.3820(3)	0.3820(3)
C	24e	0.2762(3)	0	0

they comply with the coordinates of the structural prototype $Cr_{23}C_6$. The description of the structure of $Mn_{23}C_6$ can be approached via its (rather formal) relation to the rock-salt and fluorite structures. If the structural fragment in Fig. 7A (in fact the crystallographical basis) is placed in the appropriate F-lattice so that each lattice point is occupied

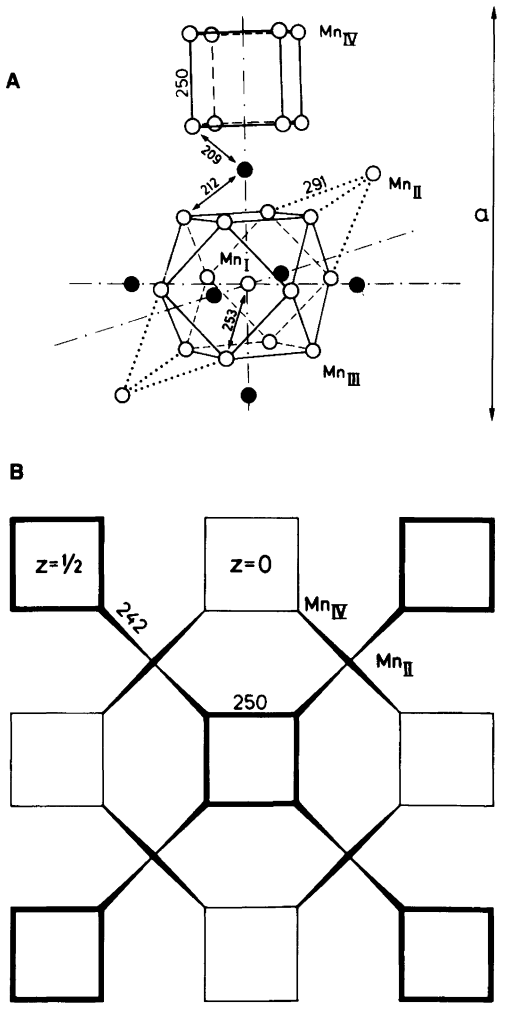

Fig. 7. Structure of $Mn_{23}C_6$. (A) Arrangement of Mn atoms and centred cuboctahedra in relation to C (filled circles). Interatomic distances (in pm at 298 K) are shown. For numbering of atoms see Table 5. (B) Projection of cube-framework of Mn_{IV} atoms interconnected with tetrahedrally coordinated Mn_{II} atoms. (The centred cuboctahedra of Mn_I and Mn_{III} are omitted.)

Table 6. Coordination (listed atom to Mn) in $Mn_{23}C_6$ and distances (in pm) at 298 K. d_{nb} = shortest contact considered as *non-bonding*, d_{span} = span of bonding contacts, d_{av} = arithmetic average of bonding contacts.

Atom	CN	d_{nb}	d_{span}	d_{av}
Mn_I	12	442	253.4 (const.)	253.4
Mn_{II}	16	437	242–291	279.0
Mn_{III}	12	358	242–291	262.2
Mn_{IV}	10	354	242–264	257.3
Mn_{av}	11.65	354	242–291	261.6
C	8	293	209.3–212.1	210.7

by the central atom of the cuboctahedron, then the cubes will occupy the octahedral (rock-salt) holes of that "close packed" structure and the Mn_{II} atoms will fill the tetrahedral (fluorite) voids. These Mn_{II} atoms are tetrahedrally coordinated to the corners of the cubes (Mn–Mn 242 pm; Fig. 7B), and are rather distant (291 pm) from the atoms of the triangular faces of the four surrounding centred cuboctahedra (which are not drawn in Fig. 7B). The square faces of the centred cuboctahedra and of the cubes are linked by carbon atoms and thus form a square anti-prismatic coordination around the C atom with an average Mn–C bond length of 211 pm. A list of averaged close contacts for the crystallographically different atoms is provided in Table 6. The closest C–C distance is 335(2) pm and cannot be attributed to any bonding interaction.

Magnetic properties. $Mn_{23}C_6$, Mn_5C_2 and Mn_7C_3 are weak paramagnets at ambient and higher temperatures. The temperature dependences of χ_g^{-1} (Fig. 8) for $Mn_{23}C_6$ and Mn_5C_2 are partly in accordance with Ref. 7.

Mn_7C_3 and Mn_5C_2 show only a slight temperature dependence in their magnetic susceptibilities. On the other hand, $Mn_{23}C_6$ follows Curie-Weiss behaviour at temperatures between $T_N = 104 \pm 3$ and 250 K, with Θ_p = $+38 \pm 3$ K and $\mu_{eff} = 1.46 \pm 0.02\ \mu_B$. Below ~75 K the susceptibility again increases.

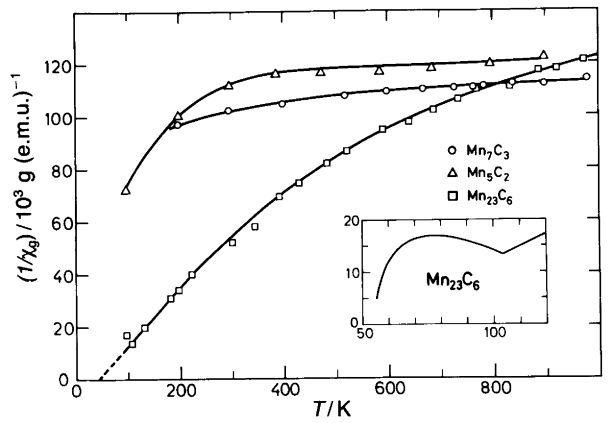

Fig. 8. Inverse magnetic susceptibility of Mn_7C_3, Mn_5C_2 and $Mn_{23}C_6$ versus temperature.

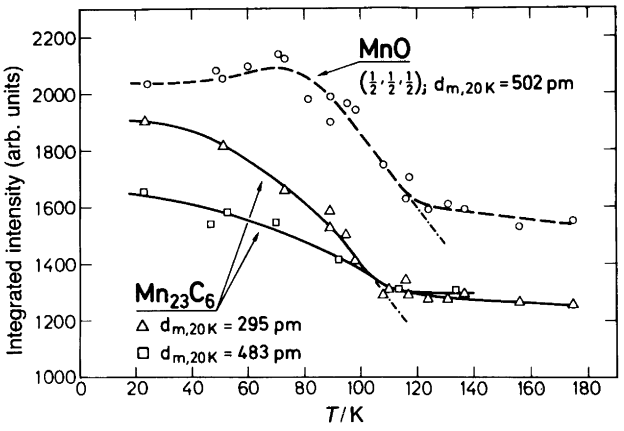

Fig. 9. Intensities of some magnetic reflections of $Mn_{23}C_6$ as function of temperature. Intensity variation for $(\frac{1}{2}, \frac{1}{2}, \frac{1}{2})$ for MnO contaminant shown for comparison.

The low-temperature neutron diffraction experiments permitted a closer look at the possibility of magnetic ordering in the manganese carbides. However, no magnetic reflections nor any magnetic contributions to the fundamental reflections were observed for Mn_5C_2 and Mn_7C_3 down to 16 K. For $Mn_{23}C_6$, some rather weak and indistinct additional peaks were found at low temperatures at diffraction angles 2θ = 22.4, 25.3, 26.9, 30.6, 33.9 and 37.1° (λ = 187.7 pm), together with contamination reflections originating from the antiferromagnetic ordering of the 3 % MnO impurity. As can be seen from Fig. 9, the magnetic reflections disappeared at $T_N = 108 \pm 5$ K, which is in agreement with the results of the magnetic susceptibility measurements. No further investigation of the magnetic structure was attempted on the basis of these few, weak and indistinct magnetic reflections.

General considerations on the structures. As is also the case for manganese metal, the structures of the manganese carbides are far more complex than those of their counterparts with metals from the beginning of the *d*-series. The manganese carbides exhibit a variety of coordination geometries, and a wide spread in the near-neighbour (bonding) distances. This large variation is somewhat surprising in view of the relatively small differences in carbon content, ranging from 20 to 30 at. % between the manganese carbides. Since there is no simple bonding description for these metallic phases, average interatomic distances are used in order to deduce some rough trends in the character of the Mn–Mn and C–Mn bonds.

The average Mn–Mn distance increases in the sequence $Mn_{23}C_6 < Mn_5C_2 < Mn_7C_3$ (cf. Tables 2, 4 and 6). One difficulty in deducing these averages is to define the limit for the maximum Mn–Mn distance which is to be considered. Nevertheless, the really interesting parameter is not the average Mn–Mn distance, but the average Mn–Mn bond

strength. It is generally accepted[34] that the relationship between bond length and bond strength can be expressed as a monotonous function in the sense that a shortened bond is taken as a token of a stronger bond. However, the actual mathematial expression of the function cannot be neglected when the *average* distances are to be compared. If there were a linear relationship, this problem would be simple. This is certainly not the case; a linear relationship would give too much weight to the longer interatomic distances which contribute little to the bond strength. Pauling[35] has proposed a logarithmic relation between bond length and bond strength in metallic phases (based, however, on C–C multiple bonds) given by eqn. (1):

$$d_s - d_n = 0.6 \log n \quad (1)$$

where d_s is the single bond distance, d_n is the actual bond distance and n is the bond order (bond strength). Using eqn. (1) it can be shown that a *geometric* average of the individually calculated bond strengths is directly proportional (by a proportionality constant k) to the bond strength calculated from the *arithmetic* average of the bond distances. Although the geometric average of the individual bond strengths is the really meaningful parameter, the much simpler arithmetic average of the bond lengths may be used for comparisons among the various carbides if the proportionality constant k is assumed to be equal or similar for these phases. The constant k depends on d_s (say, any tabulated Mn–Mn single bond distance) and on the average reciprocal coordination number $(1/CN)_{av}$ (say, of Mn in the carbide structure) according to eqn. (2):

$$k = \exp\left[(1/CN)_{av} d_s/1.38\right] \quad (2)$$

Even though the coordination number term is not exactly the same for all the three carbides, its values do not differ enough to exceed the differences between the average observed Mn–Mn bond lengths, unless extreme values for the single bond distance d_s are adopted. Hence the inference that the average Mn–Mn bond strengths decrease in sequence $Mn_{23}C_6 > Mn_5C_2 > Mn_7C_3$ seems fairly safe.

When the C–Mn interatomic distances (cf. Tables 2, 4 and 6) are discussed in the same terms, one concludes that the average C–Mn bond strength increases in the same sequence. It is hence seen that the decrease in the average Mn–Mn bond strength is (at least partly) counterbalanced by an increase in the average C–Mn bond strength. This implies an enhanced ionic contribution in the more carbon-rich manganese carbides, which indeed can be inferred from other properties, e.g. from an increase in the hydrolyzability.[10]

A comparison of the manganese carbides with Mn metal also brings out interesting features. The X-ray densities of the carbides (7.46, 7.34 and 7.38 g cm^{-3} for $Mn_{23}C_6$, Mn_5C_2 and Mn_7C_3, respectively) are comparable with that of Mn (7.48 g cm^{-3}). Closely connected with this, the average Mn–Mn distance in Mn (263.1 pm with a span of 226–293 pm, Ref. 36) is not very different from that of the manganese carbides, but the value of CN_{av} is much higher (13.1) in Mn than in the carbides. Finally, it may be remarked that the carbon atoms in the manganese carbides should not be regarded as simply interstitially added to the Mn framework, since their very presence clearly influences various crystal–chemical properties.

Acknowledgement. P.K. is grateful for the award of an exchange fellowship in 1987 under the cultural agreement between Czechoslovakia and Norway.

References

1. Starodubov, K. F. and Kolesnik, B. P. *Fiz. Metal. Materialoved. 5* (1957) 434.
2. Kuo, K. and Persson, L. E. *J. Iron Steel Inst. 178* (1954) 39.
3. Benz, R., Elliot, J. F. and Chipman, J. *Met. Trans. 4* (1973) 1449.
4. Tanaka, A. *Trans. Jpn. Inst. Metals 20* (1979) 516.
5. Aronsson, B. and Rundqvist, S. *Acta Crystallogr. 15* (1962) 878.
6. Novik, V. I. and Taran, J. N. *Izv. Akad. Nauk SSSR, Neorg. Mater. 13* (1977) 1013.
7. Domachevich, L. T., Kolotun, V. E., Kosolapova, T. Ya. and Nemchenko, V. F. *Izv. Akad. Nauk SSSR, Neorg. Mater. 13* (1977) 2173.
8. Hájek, B., Karen, P. and Brožek, V. *Collect. Czech. Commun. 48* (1983) 2740.
9. Brožek, V., Hájek, B., Karen, P., Matucha, M. and Žilka, L. *J. Radioanal. Chem. 80* (1983) 165.
10. Karen, P. and Hájek, B. *Collect. Czech. Chem. Commun. 51* (1986) 1628.
11. Westgren, A. *Jernkontorets Ann. 117* (1933) 501.
12. Stenberg, E. *Acta Chem. Scand. 15* (1961) 861.
13. Rouault, A., Herpin, P. and Fruchart, R. *Ann. Chim. (Paris) 14 (5)* (1970) 461.
14. Fruchart, R., Audière, J. P. and Michel, A. *C. R. Acad. Sci., Ser. C 266* (1968) 1691.
15. Duggin, M. J., Cox, D. and Zwell, L. *Trans. AIME 236* (1966) 1342.
16. Bouchaud, J.-P. and Fruchart, R. *C. R. Acad. Sci. 259* (1964) 160.
17. Bouchaud, J.-P. *Ann. Chim. (Paris) 14 (2)* (1967) 353.
18. Sènateur, J.-P. *Ann. Chim. (Paris) 14 (2)* (1967) 103.
19. Bowman, A. L., Arnold, G. P., Storms, E. K. and Nereson, N. G. *Acta Crystallogr., Sect. B 28* (1972) 3102.
20. Morniroli, J. P., Khachfi, M., Courtois, A., Gantois, M., Mahy, J., Van Dyck, D., Van Landuyt, J. and Amelinckx, S. *Philos. Mag., Part A 56* (1987) 93.
21. Juza, R. and Puff, H. *Z. Elektrochem. 61* (1957) 810.
22. Werner, P. E. *The Computer Programme SCANPI,* Institute of Inorganic Chemistry, University of Stockholm, Stockholm 1981.
23. Ersson, N. O. *Programme CELLKANT,* Chemical Institute, Uppsala University, Uppsala, Sweden 1981.
24. Rietveld, H. M. J. *J. Appl. Crystallogr. 1* (1968) 65.
25. Hewat, A. W. *The Rietveld Computer Program for the Profile Refinement of Neutron Diffraction Powder Patterns Modified for Anisotropic Thermal Vibrations,* UKAERE Harwell Rep. RRL 73/897, Harwell, Didcot, U.K. 1973.
26. Sears, V. F. *Thermal Neutron Scattering Lengths and Cross Sections for Condensed Matter Research,* AECL Report No. 8490, Chalk River Nucl. Lab., Ontario, Canada 1983.

27. Hilpert, S. and Paunescu, J. *Ber. Dtsch. Chem. Ges. 46* (1913) 3479.
28. Fischer, F. and Bangert, F. *Brennst. Chem. 10* (1929) 26.
29. Isobe, M. *Sci. Rept. Res. Inst. Tohoku Univ. A 3* (1951) 468; *Chem. Abstr. 47* (1953) 2585a.
30. Schuster, J. C. and Nowotny, H. *Monatsh. Chem. 111* (1980) 113.
31. Jack, K. H. *Acta Crystallogr. 5* (1952) 404.
32. Aronsson, B. *Acta Chem. Scand. 13* (1959) 109.
33. Jack, K. H. and Wild, S. *Nature (London) 212* (1966) 248.
34. Chiari, G. and Ferraris, G. *Z. Kristallogr. 191* (1990) 39.
35. Pauling, L. *J. Am. Chem. Soc. 69* (1947) 542.
36. Oberteuffer, J. A. and Ibers, J. A. *Acta Crystallogr., Sect. B 26* (1970) 1499.

Received October 3, 1990.